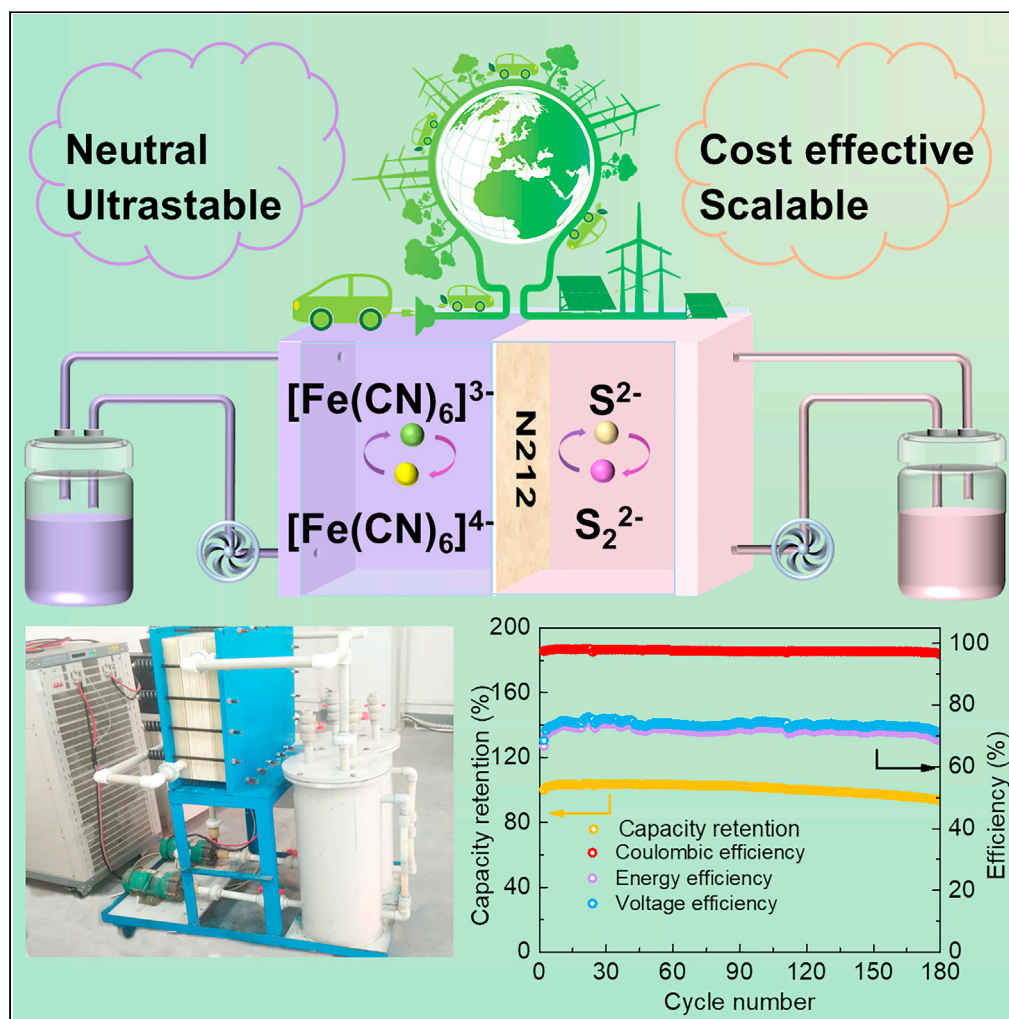


## Article

## A neutral polysulfide/ferricyanide redox flow battery



Yong Long,  
Zhizhao Xu,  
Guixiang Wang,  
..., Qijun Sun, Min  
Liu, Chuankun Jia

dingmei@csust.edu.cn (M.D.)  
jiachuankun@csust.edu.cn  
(C.J.)

**Highlights**

A neutral polysulfide/  
ferricyanide flow battery  
(PFRFB) has been  
developed

The breakthrough of  
solubility limit of  
ferricyanide/ferricyanide  
species to 1.6 M

The low-cost PFRFB  
system is ultra-high stable

The PFRFB cell stack  
shows low capacity fade  
rate of 0.021% per cycle  
(spans 60 days)

Long et al., iScience 24,  
103157  
October 22, 2021 © 2021 The  
Author(s).  
[https://doi.org/10.1016/  
j.isci.2021.103157](https://doi.org/10.1016/j.isci.2021.103157)

## Article

## A neutral polysulfide/ferricyanide redox flow battery

Yong Long,<sup>1,6</sup> Zhizhao Xu,<sup>1,6</sup> Guixiang Wang,<sup>1,6</sup> He Xu,<sup>1</sup> Minghui Yang,<sup>1</sup> Mei Ding,<sup>1,2,\*</sup> Du Yuan,<sup>1</sup> Chuanwei Yan,<sup>3</sup> Qijun Sun,<sup>4</sup> Min Liu,<sup>5</sup> and Chuankun Jia<sup>1,7,\*</sup>

## SUMMARY

**Energy storage systems are crucial in the deployment of renewable energies. As one of the most promising solutions, redox flow batteries (RFBs) are still hindered for practical applications by low energy density, high cost, and environmental concerns. To breakthrough the fundamental solubility limit that restricts boosting energy density of the cell, we here demonstrate a new RFB system employing polysulfide and high concentrated ferricyanide (up to 1.6 M) species as reactants. The RFB cell exhibits high cell performances with capacity retention of 96.9% after 1,500 cycles and low reactant cost of \$32.47/kWh. Moreover, neutral aqueous electrolytes are environmentally benign and cost-effective. A cell stack is assembled and exhibits low capacity fade rate of 0.021% per cycle over 642 charging-discharging steps (spans 60 days). This neutral polysulfide/ferricyanide RFB technology with high safety, long-duration, low cost, and feasibility of scale-up is an innovative design for storing massive energy.**

## INTRODUCTION

The global energy demand is conventionally fulfilled by fossil fuels such as coal-fired power plants and gasoline-powered vehicles. The continuous depletion of fossil fuels, as well as the arising environmental concerns like climate change caused by CO<sub>2</sub> emissions of fossil fuels, have prompted a search for “green” and sustainable renewable sources (Schrag, 2007; Chu and Majumdar, 2012; Lund, 2007; Lelieveld et al., 2019). As the cost of renewable sources such as solar and wind energy has dramatically fallen in the past decades, the highly penetration of renewable energy sources is critically dependent on large-scale energy storage systems (ESSs) which balance the intermittent production and smooth consumption (Albertus et al., 2020; Yang et al., 2011). The most significant prerequisites for widespread implementation of ESS are high safety and low cost, as well as other desirable attributes such as service lifetime, power density, and energy-density (Ziegler et al., 2019; Kwabi et al., 2020).

So far, the vast majority of energy storage technologies for the electric grid is pumped hydroelectric storage (PHS) chiefly attributed to a low cost under \$100/kWh. However, PHS approach with two huge reservoirs at different elevations is suffering from geographical and environmental constraints (Li et al., 2017). Electrochemical ESSs with appealing features of localization flexibility, scalability, efficiency, and other merits are effective alternatives (Dunn et al., 2011; Lin et al., 2015; Gür, 2018). Redox flow batteries (RFBs) allow the decoupling of energy capacity (reservoir volume and concentration of reactants) and power output (electrode area and the cell voltage) of the system by liberating the electro-active chemical species from solid electrodes inside of the electrochemical cell to liquid electrolytes stored in two outside tanks. With the merits of design flexibility, quick response time, deep-discharge capability, high efficiency, long charge/discharge cycle life etc., RFBs are highly potential solutions for massive energy storage (Ding et al., 2019; Li and Liu, 2017; Liu et al., 2019). Since the first example of RFB by pairing Fe<sup>3+</sup>/Fe<sup>2+</sup> with Cr<sup>3+</sup>/Cr<sup>2+</sup> in an acidified electrolyte (Thaller, 1976), burgeoning interests have been focused on RFBs, achieving strikingly advances. Among numerous reported RFBs, all-vanadium RFBs (VRFB) which employ the same element with different valent states as negative and positive electrolytes to mitigate crossover contamination of reactant species through the membrane (Skylas-Kazacos and Robins, 1988; Skylas-Kazacos et al., 1986) have been commercially exploited and installed in various countries (Skylas-Kazacos et al., 2010; Kear et al., 2012). However, the widespread deployment of VRFB is postponed by techno-economic concerns, such as low energy density, cell components corrosions originated from strong acidic supporting

<sup>1</sup>College of Materials Science and Engineering, Changsha University of Science & Technology, Changsha 410114, China

<sup>2</sup>National Engineering Laboratory of Highway Maintenance Technology, Changsha University of Science & Technology, Changsha 410114, China

<sup>3</sup>Institute of Metal Research, Chinese Academy of Sciences, Shenyang 110016, China

<sup>4</sup>Beijing Institute of Nanoenergy and Nanosystems, Chinese Academy of Sciences, School of Nanoscience and Technology, University of Chinese Academy of Sciences, Beijing 100049, China

<sup>5</sup>Institute of Super-microstructure and Ultrafast Process in Advanced Materials, School of Physics and Electronics, Central South University, Changsha 410083, China

<sup>6</sup>These authors contributed equally

<sup>7</sup>Lead contact

\*Correspondence: dingmei@csust.edu.cn (M.D.), jiachuankun@csust.edu.cn (C.J.)

<https://doi.org/10.1016/j.isci.2021.103157>



electrolytes and high reactants cost ascribed to the volatile price of vanadium (Hu et al., 2019a, b; Luo et al., 2019a, b; Skyllas-Kazacos et al., 2016).

Taking limited varieties and finite resources of inorganic redox species into account, organic electroactive molecules containing earth-abundant and inexpensive elemental constituents with structure diversity and property tunability have been extensively utilized as redox reactants to construct new RFBs systems.

Organic RFBs (ORFBs) either in aqueous or non-aqueous media, with advances on cell performance such as high energy density, high cell voltage, small capacity fade rate, and potential cost-effective chemistries have effectively broadened the territory of RFBs (Robb et al., 2019; Wei et al., 2014; Beh et al., 2017; Ding et al., 2018; Janoschka et al., 2015; Gong et al., 2015). However, molecular lifetime remains a critical concern for ORFBs (Kwabi et al., 2020; Brushett et al., 2020; Goulet et al., 2019; Goulet and Aziz, 2018). Due to the susceptibility to air, most ORFBs are either designed with better sealing to atmospheric oxygen or commonly operated in an argon or nitrogen filled glovebox, which raise the difficulty of operation and capital cost (Hu et al., 2019a, b; Kwabi et al., 2018). Moreover, in terms of molecular synthesis, massive scale preparations of organic electroactive materials through facile and economical routes still remain challenges toward the demands on grid-scale cell stack.

Given the drawbacks of current RFBs, it is urgent to develop new systems based on highly efficient and cost-effective electrolytes to break through the bottlenecks for practical applications. Ferricyanide  $[\text{Fe}(\text{CN})_6]^{3-}$ , and its reduced form  $[\text{Fe}(\text{CN})_6]^{4-}$ , with well-defined reversible redox properties, high stability and low cost, are attractive positive candidates of RFBs, e.g., first utilization of  $\text{K}_4[\text{Fe}(\text{CN})_6]$  in a semi-flow alkaline RFB (Adams, 1979; Koshel et al., 1995). Recently, ferricyanide/ferricyanide couple has been extensively employed in combination with various organic electroactive reactants (Lin et al., 2015, 2016; Kwabi et al., 2018; Yang et al., 2018; Hong et al., 2014) such as quinone-, anthraquinone-, and alloxazine-based anolytes. The fundamental properties and electrochemical kinetics of  $\text{K}_3[\text{Fe}(\text{CN})_6]$  and  $\text{K}_4[\text{Fe}(\text{CN})_6]$  in various supporting electrolytes with different pH values were explored (Luo et al., 2017). Particularly, the pH-dependent cycling stability of ferricyanide/ferricyanide based RFBs were investigated and the redox couple functioned best at neutral or near neutral conditions. However, the concentration of ferricyanide/ferricyanide catholyte was commonly less than 0.8 M, which caused an ultra-low energy density of above reported RFBs. To address the challenge of low solubility limit,  $(\text{NH}_4)_3[\text{Fe}(\text{CN})_6]$  with high solubility (1.6 M) was synthesized via a cation modulation strategy and employed as the catholyte to construct RFBs (Luo et al., 2019a, b). Concerning on the cost and mass-production of reactants toward electric-grid energy storage, commercially available  $\text{K}_4[\text{Fe}(\text{CN})_6]$  with a low cost of \$2.5 per kg is judiciously chosen as cathodic energy storage material in this work. Furthermore, inspired by the results that the mixed cations of ferricyanide could improve the solubility illustrated by the earlier patent (Esswein et al., 2014), a similar approach was employed in this work to resolve the fundamental solubility issue of ferrocyanide (up to 1.6 M) species in neutral electrolyte.

On the other hand, sulfur, widely known to be dissolved in the form of polysulfide with inherent merits of abundance, low cost, high solubility, and high theoretical capacity, has attracted much attention on lithium-sulfur battery RFBs (Rauh et al., 1979; Lochala et al., 2017), potassium-sulfur battery (Lu et al., 2015) and polysulfide/halide (Price et al., 1999; Wei et al., 2015; Zhang et al., 2019; Ma et al., 2019; Zhou et al., 2020; Li et al., 2016; Li and Lu, 2021). Among which, the polysulfide/iodide RFB, which possessed a high-energy density and low materials cost, still suffered from severe cross-over, side reactions of iodide, and the increased extra cost of Nafion membrane (Li et al., 2016). Recently, an original charge-reinforced ion selectivity membrane was fabricated to restrain the crossover of reactants and ameliorate the migration of water, strikingly prolonging the lifespan of polysulfides/iodide RFB (Li and Lu, 2021). To provide a promising anodic alternative to couple with the ferricyanide/ferricyanide cathodic side, we choose  $\text{K}_2\text{S}$  with high solubility and vast availability at low cost. For the proposed polysulfide/ferricyanide redox flow battery (PFRFB) system (Figure 1A), the redox reactants are ultra-abundant and the KCl supporting electrolytes are non-corrosive neutral solutions. According to assessment methods and performance metrics summarized for RFBs (Yao et al., 2021), the present PFRFB exhibits high cell performances with capacity retention of 96.9% after 1,500 cycles (equivalent to a capacity fade rate of 0.002%/cycle or 0.10%/day) and low chemical cost of \$32.47/kWh. Further, to verify the practical scalability of the proposed system, a stack consisting of 10 cells with active geometrical area of  $1700 \text{ cm}^2$  is pioneeringly assembled and investigated, demonstrating an excellent capacity fade rate of 0.021%/cycle over 642 charging-discharging steps (span for 60 days).

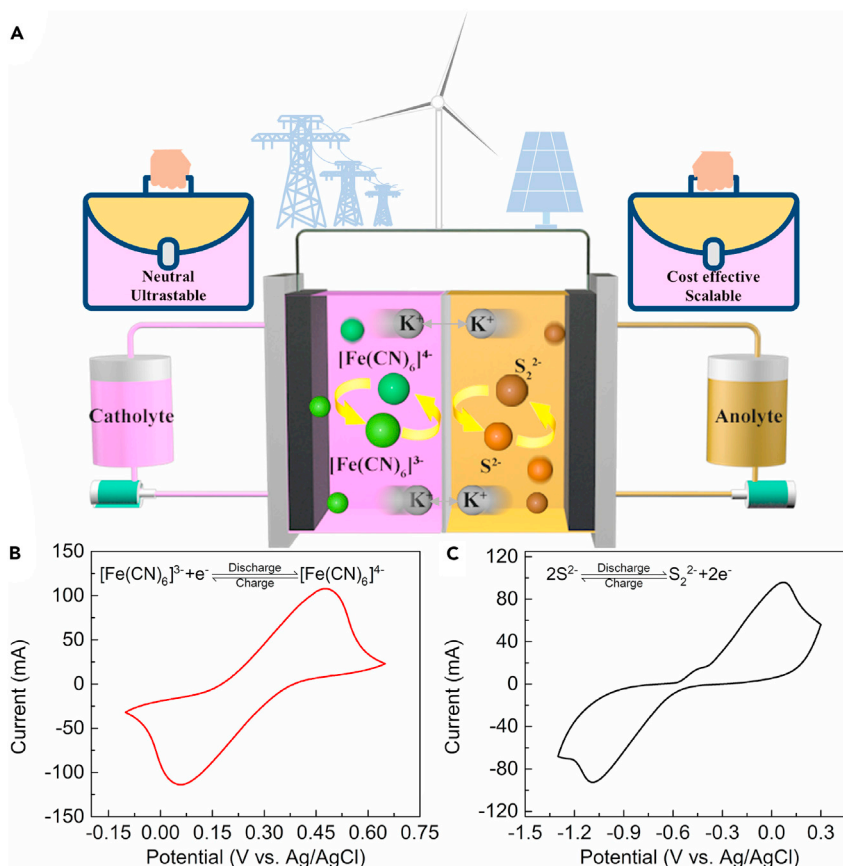


**Figure 1. Concept of the neutral polysulfide/ferricyanide redox flow battery (PFRFB) full cell and cyclic voltammograms of the redox couples**

(A) Schematic illustration of the proposed PFRFB system in this work.

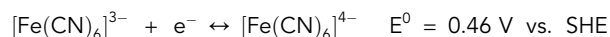
(B) Cyclic voltammograms of ferricyanide/ferrocyanide with 1.0 M KCl as supporting electrolyte under a scan rate of  $50 \text{ mV s}^{-1}$ .

(C) Cyclic voltammograms of sulfide/polysulfide in 1.0 M KCl solution under a scan rate of  $50 \text{ mV s}^{-1}$ .

## RESULTS AND DISCUSSION

### Electrochemical characteristics of redox reactants

To verify the reversible electrochemical reactions in the designed PFRFB, cyclic voltammetry (CV) measurements were conducted. A solution of 0.1 M  $\text{K}_3[\text{Fe}(\text{CN})_6]$  in 1.0 M KCl was scanned at  $50 \text{ mV s}^{-1}$  within the potential window between  $-0.1 \text{ V}$  and  $0.65 \text{ V}$ . As shown in Figure 1B, a pair of reversible redox peaks was revealed and the corresponding redox reaction was described as:



Similarly, a solution with 0.1 M  $\text{K}_2\text{S}$  in 1.0 M KCl was scanned at  $50 \text{ mV s}^{-1}$  with the potential ranging from  $-1.3 \text{ V}$  to  $0.3 \text{ V}$ . Apparently, one pair of redox peaks with higher peak current densities appear accompanied with minor visualized peaks (Figure 1C). As previously noted, aqueous polysulfide solutions contain multiple species involving the simultaneous equilibria. In this study, a  $\text{K}_2\text{S}$  electrolyte refers to a solution nominally composed of dissolved  $\text{K}_2\text{S}$  solution. And the main redox reaction was ascribed to the reduction of dissolved  $\text{S}^{2-}$  (predominant) to  $\text{S}_2^{2-}$  by the following simplified process:



Given the aforementioned redox reactions, the formal-potential difference between the ferricyanide/ferrocyanide and  $\text{S}^{2-}/\text{S}_2^{2-}$  redox pairs is 0.97 V.

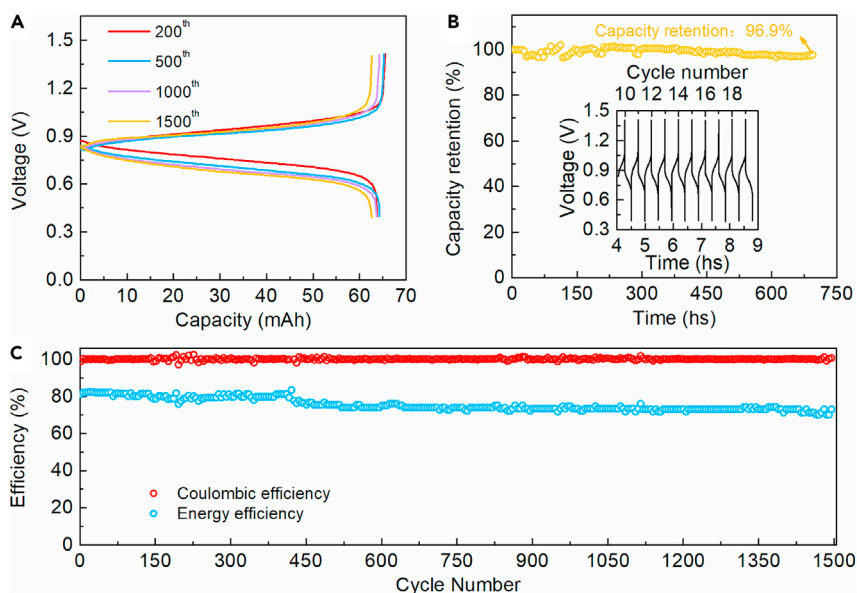


**Figure 2. Electrochemical performance of the PFRFB cell**

All measurements were conducted with a cell comprised of a 25.0 mL solution of 0.1 M  $K_3[Fe(CN)_6]$  + 2.0 M KCl as the catholyte and a 15.0 mL solution of 2.0 M  $K_2S$  + 1.0 M KCl as the anolyte at a current density of  $20 \text{ mA cm}^{-2}$ .

(A) Selected cell voltage profiles of the PFRFB cell during charging-discharging tests.

(B) Galvanostatic capacity retention of the cell over time. The insert is selected charging and discharging curves from the 10<sup>th</sup> cycle to the 20<sup>th</sup> cycle over time.

(C) Coulombic efficiency and energy efficiency of the cell as a function of cycle numbers.

CV curves of the two redox pairs at different sweeping rates ranging from  $1 \text{ mV s}^{-1}$  to  $50 \text{ mV s}^{-1}$  were recorded to quantify the kinetic characteristics of redox species (Figure S1, Tables S1 and S2). Linear relationships of both the oxidation and reduction peak current densities with the square root of scan rates reveal redox reactions are standard diffusion-controlled processes. The calculated diffusion coefficients of  $[Fe(CN)_6]^{3-}/[Fe(CN)_6]^{4-}$  and  $S_2^{2-}/S_2^{2-}$  in the KCl electrolyte at room temperature were  $4.1 \times 10^{-6} \text{ cm}^2 \text{ s}^{-1}$  and  $2.8 \times 10^{-6} \text{ cm}^2 \text{ s}^{-1}$ , respectively, which are comparable with the reported values (Li et al., 2016; Gong et al., 2016).

### Cell performance of the neutral PFRFB

To confirm the electrochemical reversibility and long timescale cycling stability of cathodic and anodic redox reactants, a neutral PFRFB cell was designed and assembled. Either charging or discharging curve shows only one plateau (Figure 2A), which corresponds to the redox reactions revealed by the CV and verifies that no more polysulfide species than  $S_2^{2-}$  dominate at the anolyte side. For 200 consecutive cycles, the discharging capacity of the cell remains 95.07% of the theoretical capacity, revealing high energy conversion efficiency. After extended cycling tests, very limited deviation of discharging capacity for the 1500<sup>th</sup> cycles is observed, suggesting ultra-high capacity retention and excellent stability. The narrow separations between the charging curves and immediately preceding discharging curves indicate a mild ohmic polarization with a small IR drop observed from the 200<sup>th</sup> cycle to the 1500<sup>th</sup> cycle. A capacity retention of up to 96.9% over 1,500 cycles (equivalent to a capacity fade rate of 0.002%/cycle, one-month duration) clearly indicates the remarkable cycling stability of the cell (Figure 2B), which is among the best cycling performances of reported RFBs. At the initial cycling, the coulombic efficiency (CE) and energy efficiency (EE) are 98.63% and 80.95%, respectively (Figure 2C). The CE retains unprecedented stable during the long-time cycling tests and even reaches a higher value of 99.76% at the 1500<sup>th</sup> cycle, delivering the ultra-high cycling stability of the cell attributed to the high chemical and electrochemical stability. Note that the slight increase in the CE could be ascribed to the conditioning of the carbon felt electrodes that the increased hydrophobicity/wettability after initial cycles reduces the charge-transfer and the interfacial resistances (Li et al., 2016; Zhao et al., 2014). After continuous charging-discharging operations, EE sluggishly drops to 70.00% at the end of 1500<sup>th</sup> cycle which is perhaps correlated with the increase of area-specific resistance of the membrane. This speculation is evidenced by the appearance of traces of light-yellow

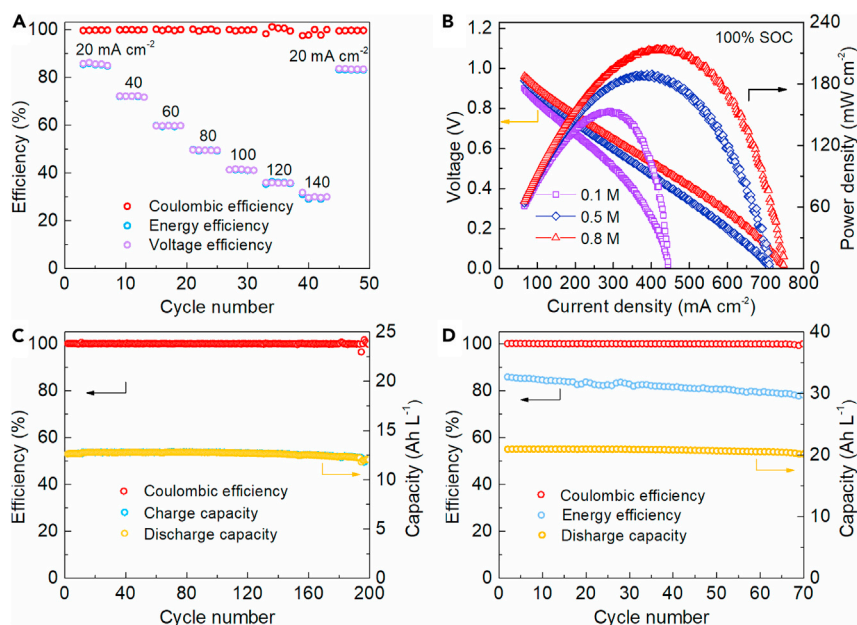


**Figure 3. Electrochemical performance of the PFRFB cells with different concentration combinations of electrolytes**

(A) Rate performance of the cell with a 25.0 mL solution of 0.1 M  $K_3[Fe(CN)_6]$  + 2.0 M KCl as the catholyte and a 15.0 mL solution of 2.0 M  $K_2S$  + 1.0 M KCl as the anolyte at different current densities.

(B) Polarization curves of PFRFB cells consisting of a 25.0 mL solution of ferricyanide at various concentrations (0.1 M, 0.5 M and 0.8 M, respectively) + 2.0 M KCl as catholyte in combination with a 15.0 mL solution of 2.0 M  $K_2S$  + 1.0 M KCl as anolyte.

(C) Coulombic efficiency and volumetric capacity of a PFRFB cell comprised of a 25.0 mL solution of 0.5 M  $K_3[Fe(CN)_6]$  + 2.0 M KCl as the catholyte and a 25.0 mL solution of 2.0 M  $K_2S$  + 1.0 M KCl as anolyte at a current density of 50 mA cm<sup>-2</sup>.

(D) Coulombic efficiency, energy efficiency and volumetric capacity of a PFRFB cell combined a 25.0 mL solution of 0.8 M  $K_3[Fe(CN)_6]$  + 0.5 M KCl as catholyte, with a 40.0 mL solution of 2.0 M  $K_2S$  + 1.0 M KCl as anolyte at a current density of 20 mA cm<sup>-2</sup>.

precipitate on the anolyte facing-side of the membrane, observed in the disassembled cell after cycling tests. In this work, as the catholyte is capacity-limiting-side, the formation of non-valent sulfur precipitate (ascribed to side reactions of dissolved (poly)sulfide species in the anolyte) has negligible influences on capacity retention and CE of the cell. Moreover, it is conspicuous from the optical spectra (Figure S2) that the catholyte exhibits high stability during the cycling process.

To evaluate the effects of current densities on the cell performance, the rate performance was studied (Figure 3A). The cell delivers nearly constant CE which are higher than 95.0% under all applied current densities, indicating high stability and electrochemical reversibility of redox reactants at both sides. The voltage efficiency (VE), as well as the EE decrease strikingly with the increment of current density from 20 mA cm<sup>-2</sup> to 140 mA cm<sup>-2</sup> at an interval of 20 mA cm<sup>-2</sup>, indicating reservoirs with bigger size are required for larger power output. Despite the above case, the ultra-long cycling stability and mild operation condition at neutral pH media could offset the cost increment for sizing up the tanks at set-up stage, which can synergistically facilitate the industrialization of PFRFBs.

The correlation between ferricyanide concentration and cell performance is further investigated. As shown in Figure 3B, polarization curves illustrate the galvanostatic peak power density scales up with the rising concentration of capacity-limiting-side electrolyte. By employing a ferricyanide-containing solution with different concentrations of 0.1 M, 0.5 M and 0.8 M approaching the solubility limit of  $K_3[Fe(CN)_6]$  at room temperature, the peak power density increases from 153.4 mW cm<sup>-2</sup> at 292.4 mA cm<sup>-2</sup>, to 189.3 mW cm<sup>-2</sup> at 403.0 mA cm<sup>-2</sup>, and further to 213.9 mW cm<sup>-2</sup> at 417.6 mA cm<sup>-2</sup>. The voltage and current density under higher concentration conditions follow a typical ohmic relationship, indicating the voltage loss chiefly assigned to the internal resistance. Contrarily, at the low concentration, both ohmic

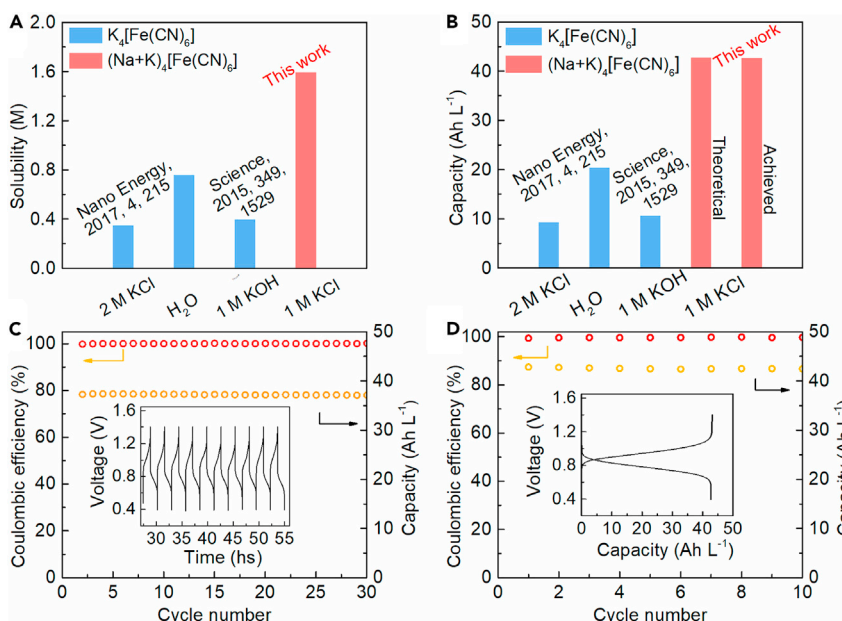


**Figure 4. Strategies for improving solubility limits of  $[\text{Fe}(\text{CN})_6]^{4-}$  and cell performance employing concentrated- $[\text{Fe}(\text{CN})_6]^{4-}/\text{S}_2^{2-}$  pair at neutral solution**

- (A) Enhancement of solubility limit of  $[\text{Fe}(\text{CN})_6]^{4-}$  by adopting a equimolar mixture of  $\text{K}_4[\text{Fe}(\text{CN})_6]$  and  $\text{Na}_4[\text{Fe}(\text{CN})_6]$  in 1.0 M KCl solution at room temperature.
- (B) Specific capacity improvement of a PFRFB cell in which the catholyte with 1.6 M  $[\text{Fe}(\text{CN})_6]^{4-}$  fulfilled by a mixture of 0.8 M  $\text{K}_4[\text{Fe}(\text{CN})_6]$  and 0.8 M  $\text{Na}_4[\text{Fe}(\text{CN})_6]$  is the capacity-limiting-side.
- (C) Cell performance of a PFRFB cell at a current density of  $50 \text{ mA cm}^{-2}$  with a 10.0 mL concentrated-solution of 1.4 M  $[\text{Fe}(\text{CN})_6]^{4-}$  fulfilled by a equimolar mixture of  $\text{K}_4[\text{Fe}(\text{CN})_6]$  and  $\text{Na}_4[\text{Fe}(\text{CN})_6]$  in 1.0 M KCl as catholyte and a 90.0 mL solution of 2.0 M  $\text{K}_2\text{S}$  + 1.0 M KCl as anolyte. Insert: Selected voltage profiles versus time during charging-discharging process.
- (D) Cell performance of a PFRFB cell at a current density of  $50 \text{ mA cm}^{-2}$  with a 10.0 mL concentrated-solution of 1.6 M  $[\text{Fe}(\text{CN})_6]^{4-}$  employing a equimolar mixture of  $\text{K}_4[\text{Fe}(\text{CN})_6]$  and  $\text{Na}_4[\text{Fe}(\text{CN})_6]$  in 1.0 M KCl as catholyte and a 90.0 mL solution of 3.0 M  $\text{K}_2\text{S}$  in 1.0 M KCl. Insert: Selected charging-discharging curves.

polarization and concentration polarization coexist and contribute to the voltage loss, which are evidenced by the discrepancy from the linear correlation of voltage versus the current density. Galvanostatic charging/discharging profiles of the proposed neutral PFRFB cells with various initial concentrations of ferricyanide were exploited (Figures 3C and 3D). Both cells with solutions of 0.5 M  $\text{K}_3[\text{Fe}(\text{CN})_6]$  + 2.0 M KCl and 0.8 M  $\text{K}_3[\text{Fe}(\text{CN})_6]$  + 0.5 M KCl, respectively, in the positive side achieve very high values of CE (>96.0%) without visible drop over the cycling process, indicating high stability of the electroactive reactants. Although the capacity retentions up to approximate 100% are very high at the initial cycles, faster capacity fade suggests more severe voltage loss due to the undesired side reactions at higher concentration conditions.

The energy density of RFBs is determined by either the catholyte or the anolyte, whichever is limited. As reported, the concentration of metal polysulfides anolyte was up to 12.0 M (Li et al., 2017). Herein, the saturated concentrations of  $\text{K}_2\text{S}$  in both  $\text{H}_2\text{O}$  and 1.0 M KCl solution were measured. Apparently, the solubility limit for  $\text{K}_2\text{S}$  was approximate 8.0 M in 1.0 M KCl solution. As a result, the theoretical energy density of  $\text{K}_2\text{S}$  in 1.0 M KCl solution could reach to a high value of  $208.0 \text{ Wh L}^{-1}$ . On the other hand, the solubility of  $\text{K}_4[\text{Fe}(\text{CN})_6]$  ( $\text{K}_4$ ) in both neutral and alkaline supporting electrolytes is lower than  $\text{K}_3[\text{Fe}(\text{CN})_6]$  ( $\text{K}_3$ ), indicating that  $\text{K}_4$  is the preferred electroactive reactant in a RFB cell due to its low solubility limit. In addition, as shown in Figure 4A, the concentration of  $\text{K}_4$  in alkaline solution (0.40 M) is higher than that in neutral solution (0.35 M), therefore, the volumetric capacity of RFB with  $\text{K}_3/\text{K}_4$  catholyte is only  $\sim 10 \text{ Ah L}^{-1}$  (Figure 4B) and still hindered by the low concentration of  $\text{K}_4$  (0.4 M). Importantly, the practical application of  $\text{K}_3/\text{K}_4$  based RFBs should improve the solubility of  $\text{K}_3/\text{K}_4$ . In this work, based on the neutral solution with KCl as the supporting electrolyte, a sophisticated mixture of  $\text{K}_4[\text{Fe}(\text{CN})_6]$  and  $\text{Na}_4[\text{Fe}(\text{CN})_6]$  was employed to obtain a high concentrated-solution of the redox couples of  $[\text{Fe}(\text{CN})_6]^{4-}/[\text{Fe}(\text{CN})_6]^{3-}$ . A maximum concentration value of 1.6 M of  $[\text{Fe}(\text{CN})_6]^{4-}$  can be readily achieved at room temperature which breaks through the

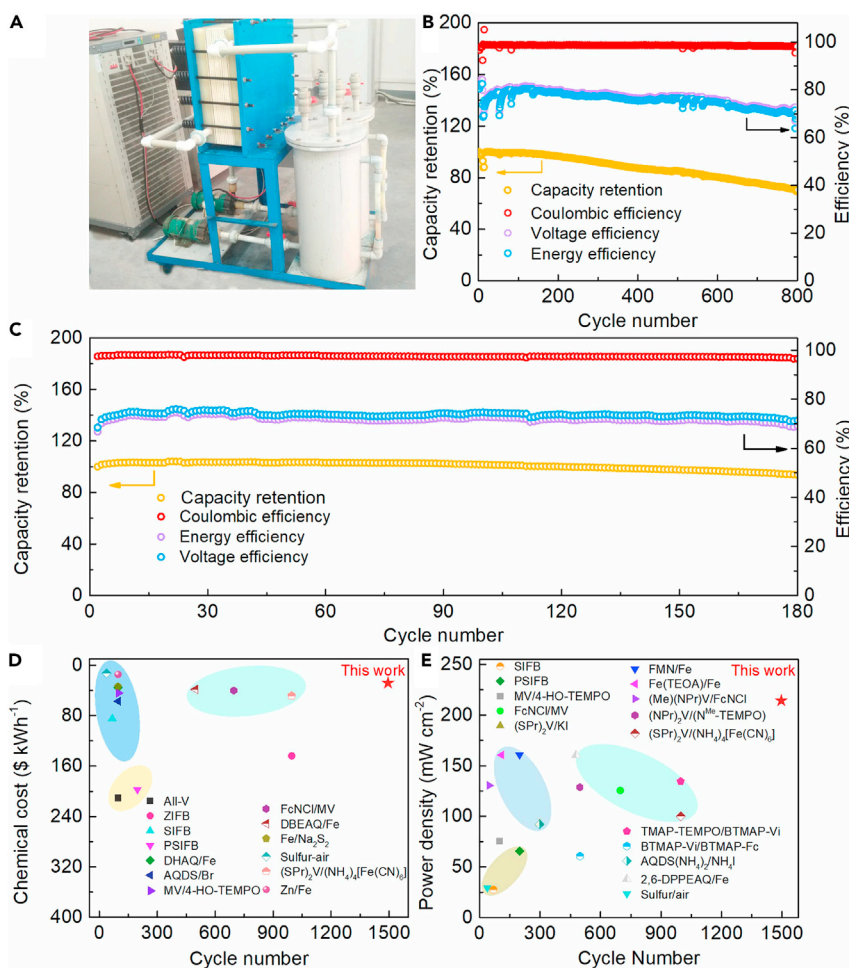


**Figure 5. Electrochemical performance of the PFRFB stack and a summary of the chemical cost and power density of various reported RFBs**

(A) A photograph of the cell stack employing  $K_3[Fe(CN)_6]/K_2S$  as redox active species proposed in the present work. (B) Electrochemical performance of the cell stack consisting of a 20.0 L solution of 0.2 M  $K_3[Fe(CN)_6]$  + 1.0 M KCl as the catholyte and a 20.0 L solution of 1.0 M  $K_2S$  + 1.0 M KCl as the anolyte under 34 A. (C) Electrochemical performances of the cell stack consisting of a 20.0 L solution of 0.5 M  $K_3[Fe(CN)_6]$  + 1.0 M KCl as the catholyte and a 20.0 L solution of 1.0 M  $K_2S$  + 1.0 M KCl as the anolyte at a current of 51 A. (D) A summary of the chemical cost of PFRFB in this work with respect to various reported RFB systems. (E) Comparisons of power density output among various prior reported RFB work.

fundamental solubility limit (Figures 4A and S3). Specific capacity of a PFRFB cell based on the catholyte of 1.6 M  $[Fe(CN)_6]^{4-}$  in 1.0 M KCl solution was greatly improved (Figure 4B). The achieved specific capacity ( $42.8 \text{ Ah L}^{-1}$ ) is close to the theoretical value ( $42.9 \text{ Ah L}^{-1}$ ), implying excellent electrochemical activity and reversibility of this mixed  $[Fe(CN)_6]^{4-}$  catholyte. Besides, CE of the cells with 1.4 M  $[Fe(CN)_6]^{4-}$  and 1.6 M  $[Fe(CN)_6]^{4-}$  in the catholyte, respectively, maintain stable and high values during the cycling processes (Figures 4C and 4D) indicating good stability of ultra-high concentrated  $[Fe(CN)_6]^{4-}$  mixed catholyte. The present work demonstrates that the cell performance can be significantly enhanced by concentrating the  $[Fe(CN)_6]^{4-}$ .

### Electrochemical performance of the cell stack

To verify the practical scalability of the proposed neutral PFRFB system, cell stacks with various concentration combinations of  $K_3[Fe(CN)_6]$  and  $K_2S$  were assembled and electrochemically investigated (Figure 5A). Thereinto, the cell stack consisting of a 20.0 L solution of 0.2 M  $K_3[Fe(CN)_6]$  in 1.0 M KCl as the catholyte and a 20.0 L solution of 1.0 M  $K_2S$  in 1.0 M KCl as the anolyte exhibits high cycling stability with a low capacity

fade rate of 0.021%/cycle (Figure 5B). Moreover, under the current of 34 A over 642 repetitive charging-discharging cycles (approximate 50 days), the nearly invariant high values of CE above 97.40%, as well as slightly fluctuating values of VE and EE around 82.86% and 80.97%, strongly support the high stability and excellent performances of the cell stack. Furthermore, the cycling performance of the cell stack with more concentrated catholyte shows a low capacity fade rate of 0.056%/cycle and high CE of an average value 97.55% over 204 galvanostatic charging-discharging cycles (spans 20 days) under a current of 51 A, indicating the reliability for practical applications of the cell stack based on the proposed neutral PFRFB system (Figure 5C).

Last but not the least, another prerequisite of batteries for commercialization is the effective cost. The techno-economic analysis shows installed cost of this approach is comparable with PHS and CAES, which is highly promising for massive penetration of intermittent renewable electricity. The proposed neutral PFRFB approach demonstrates a significantly lower materials cost of \$32.47/kWh with respect to the state-of-art vanadium-based RFBs of \$124.40/kWh (Ziegler et al., 2019) and other recently proposed RFB systems (Figure 5D). Besides, the neutral operating condition also dramatically reduces the system cost and maintenance fee. In the present study, Nafion 212 membrane was employed as the separator, which is anticipated to be replaced with cheaper homemade membrane under the mild neutral condition and believed to be capable of further decreasing the system cost.

### Conclusions

In combination with the inherent electrochemical stability, reversibility and the low wholesale-price of potassium ferricyanide and potassium sulfide, we demonstrate a neutral PFRFB system. The proposed cell delivers a superior high capacity retention and CE over ultra-long-time cycling of 1,500 cycles (one-month testing time), as well as high power density output (Figure 5E). Besides high cell performance at laboratory scale, a cell stack consisting of 10 pieces of single cell with effective geometric membrane area of 1700 cm<sup>2</sup> reveals the high stability and practicability of the proposed systems. The achieved high CE and low capacity fade rate for 642 cycles (spans almost 2 months) promote this approach in decadal operation for potential grid-scale energy storage in near future. Moreover, the neutral PFRFB system demonstrates a significantly low materials cost which is benefit for an expected low system cost. With the demonstrated high stability, robust battery performance, inherent low material cost, highly scalable and environmental benign natures, the neutral PFRFB offers a facile solution for sustainable and economical energy storage strategy.

### Limitations of the study

In the current study, carbon felt without any catalyst coating was used as electrodes. In combination with the sluggish kinetics of redox reactions of polysulfide species, the power density of the proposed PFRFB was still in need of improvement for practical applications. With high-efficient catalyst modified electrode toward the polysulfide species, the power density of this RFB system will be much boosted in the coming work.

### STAR★METHODS

Detailed methods are provided in the online version of this paper and include the following:

- KEY RESOURCES TABLE
- RESOURCE AVAILABILITY
  - Lead contact
  - Materials availability
  - Data and code availability
- EXPERIMENTAL MODEL AND SUBJECT DETAILS
- METHOD DETAILS
  - Cell construction and stack assembly
  - Electrochemical characterizations
- QUANTIFICATION AND STATISTICAL ANALYSIS
- ADDITIONAL RESOURCES

### SUPPLEMENTAL INFORMATION

Supplemental information can be found online at <https://doi.org/10.1016/j.isci.2021.103157>.

## ACKNOWLEDGMENTS

We acknowledge financial support from the 100 Talented Team of Hunan Province (XiangZu [2016] 91), the “Huxiang high-level talents” program (2019RS1046 and 2018RS3077) and the Open Fund of National Engineering Laboratory of Highway Maintenance Technology (Changsha University of Science & Technology) (kfj170105).

## AUTHOR CONTRIBUTIONS

M.D. and C.J. conceived the idea and supervised the work. Y.L., Z.X., and G.W. carried out the experiments. M.D., Y.L., and C.J. cowrote the paper. All authors discussed the results and comments on the manuscript.

## DECLARATION OF INTERESTS

The authors declare no competing interests.

Received: May 3, 2021

Revised: September 8, 2021

Accepted: September 17, 2021

Published: October 22, 2021

## REFERENCES

- Adams, G.B. (1979). US Pat. 4, 180 623.
- Albertus, P., Manser, J.S., and Litzelman, S. (2020). Long-duration electricity storage applications, economics, and technologies. *Joule* 4, 21–32.
- Beh, E.S., Porcellinis, D.D., Gracia, R.L., Xia, K.T., Gordon, R.G., and Aziz, M.J. (2017). A neutral pH aqueous organic–organometallic redox flow battery with extremely high capacity retention. *ACS Energy Lett* 2, 639–644.
- Brushett, F.R., Aziz, M.J., and Rodby, K.E. (2020). On lifetime and cost of redox-active organics for aqueous flow batteries. *ACS Energy Lett.* 5, 879–884.
- Chu, S., and Majumdar, A. (2012). Opportunities and challenges for a sustainable energy future. *Nature* 488, 294–303.
- Ding, Y., Zhang, C., Zhang, L., Zhou, Y., and Yu, G. (2018). Molecular engineering of organic electroactive materials for redox flow batteries. *Chem. Soc. Rev.* 47, 69–103.
- Ding, Y., Zhang, C., Zhang, L., Zhou, Y., and Yu, G. (2019). Pathways to widespread applications: development of redox flow batteries based on new chemistries. *Chem* 5, 1964–1987.
- Dunn, B., Kamath, H., and Tarascon, J.-M. (2011). Electrical energy storage for the grid: a battery of choices. *Science* 334, 928–935.
- Esswein, A.J., Goeltz, J., and Amadeo, D. (2014). High Solubility Iron Hexacyanides, US Patent 2014/0051003 A1 (2/20/2014 2014), filed May 6, 2013, and Granted Mar 27, 2018.
- Gong, K., Fang, Q., Gu, S., Li, S.F.Y., and Yan, Y. (2015). Nonaqueous redox-flow batteries: organic solvents, supporting electrolytes, and redox pairs. *Energy Environ. Sci.* 8, 3515–3530.
- Gong, K., Xu, F., Grunewald, J.B., Ma, X., Zhao, Y., Gu, S., and Yan, Y. (2016). All-soluble all-iron aqueous redox-flow battery. *ACS Energy Lett.* 1, 89–93.
- Goulet, M.-A., and Aziz, M.J. (2018). Flow battery molecular reactant stability determined by symmetric cell cycling methods. *J. Electrochem. Soc.* 165, A1466–A1477.
- Goulet, M.-A., Tong, L., Pollack, D.A., Tabor, D.P., Odom, S.A., Aspuru-Guzik, A., Kwan, E.E., Gordon, R.G., and Aziz, M.J. (2019). Extending the lifetime of organic flow batteries via redox state management. *J. Am. Chem. Soc.* 141, 8014–8019.
- Gür, T.M. (2018). Review of electrical energy storage technologies, materials and systems: challenges and prospects for large-scale grid storage. *Energy Environ. Sci.* 11, 2696–2767.
- Hong, J., Lee, M., Lee, B., Seo, D.-H., Park, C.B., and Kang, K. (2014). Biologically inspired pteridine redox centres for rechargeable batteries. *Nat. Commun.* 5, 5335–5343.
- Hu, B., Luo, J., DeBruler, C., Hu, M., Wu, W., and Liu, L.T. (2019a). Redox-active inorganic materials for redox flow batteries. In *Encyclopedia of Inorganic and Bioinorganic Chemistry*, 3, H. Wang and B.P.T. Fokwa, eds. (Wiley), pp. 211–235.
- Hu, B., Luo, J., Hu, M., Yuan, B., and Liu, T.L. (2019b). A pH-neutral, metal-free aqueous organic redox flow battery employing an ammonium anthraquinone anolyte. *Angew. Chem. Int. Ed.* 58, 16629–16636.
- Janoschka, T., Martin, N., Martin, U., Friebe, C., Morgenstern, S., Hiller, H., Hager, M.D., and Schubert, U.S. (2015). An aqueous, polymer-based redox-flow battery using non-corrosive, safe, and low-cost materials. *Nature* 527, 78–81.
- Kear, G., Shah, A.A., and Walsh, F.C. (2012). Development of the all-vanadium redox flow battery for energy storage: a review of technological, financial and policy aspects. *Int. J. Energy. Res.* 36, 1105–1120.
- Koshel, N.D., Zvyachynyi, V.G., and Zaderei, N.D. (1995). Characteristics of redox batteries based on the zinc-ferricyanide system. *Russ. J. Electrochem.* 30, 443–446.
- Kwabi, D.G., Ji, Y., and Aziz, M.J. (2020). Electrolyte lifetime in aqueous organic redox flow batteries: a critical review. *Chem. Rev.* 120, 6467–6489.
- Kwabi, D.G., Lin, K., Ji, Y., Kerr, E.F., Goulet, M.-A., Porcellinis, D.D., Tabor, D.P., Pollack, D.A., Aspuru-Guzik, A., Gordon, R.G., et al. (2018). Alkaline quinone flow battery with long lifetime at pH 12. *Joule* 2, 1894–1906.
- Lelieveld, J., Klingmüller, K., Pozzer, A., Burnett, R.T., Haines, A., and Ramanathan, V. (2019). Effects of fossil fuel and total anthropogenic emission removal on public health and climate. *Proc. Natl. Acad. Sci. U S A* 116, 7192–7197.
- Li, B., and Liu, J. (2017). Progress and directions in low-cost redox-flow batteries for large-scale energy storage. *Natl. Sci. Rev.* 4, 91–105.
- Li, Z., and Lu, Y.-C. (2021). Polysulfide-based redox flow batteries with long life and low leveled cost enabled by charge-reinforced ion-selective membranes. *Nat. Energy* 6, 517–528.
- Li, Z., Pan, M.S., Su, L., Tsai, P.-C., Badel, A.F., Valle, J.M., Eiler, S.L., Xiang, K., Brushett, F.R., and Chiang, Y.-M. (2017). Air-breathing aqueous sulfur flow battery for ultralow-cost long-duration electrical storage. *Joule* 1, 306–327.
- Li, Z., Weng, G., Zou, Q., Cong, G., and Lu, Y.-C. (2016). A high-energy and low-cost polysulfide/iodide redox flow battery. *Nano Energy* 30, 283–292.
- Lin, K., Chen, Q., Gerhardt, M.R., Tong, L., Kim, S.B., Eisenach, L., Valle, A.W., Hardee, D., Gordon, R.G., Aziz, M.J., and Marshak, M.P. (2015). Alkaline quinone flow battery. *Science* 349, 1529–1532.
- Lin, K., Gómez-Bombarelli, R., Beh, E.S., Tong, L., Chen, Q., Valle, A., Aspuru-Guzik, A., Aziz, M.J., and Gordon, R.G. (2016). A redox-flow battery

- with an alloxazine-based organic electrolyte. *Nat. Energy* 1, 16102–16109.
- Liu, W., Lu, W., Zhang, H., and Li, X. (2019). Aqueous flow batteries: research and development. *Chem. Eur. J.* 25, 1649–1664.
- Lochala, J., Liu, D., Wu, B., Robinson, C., and Xiao, J. (2017). Research progress toward the practical applications of lithium–sulfur batteries. *ACS Appl. Mater. Inter.* 9, 24407–24421.
- Lu, X., Bowden, M.E., Sprenkle, V.L., and Liu, J. (2015). A low cost, high energy density, and long cycle life potassium–sulfur battery for grid-scale energy storage. *Adv. Mater.* 27, 5915–5922.
- Luo, J., Hu, B., Debruler, C., Bi, Y., Zhao, Y., Yuan, B., Hu, M., Wu, W., and Liu, T.L. (2019a). Unprecedented capacity and stability of ammonium ferrocyanide catholyte in pH neutral aqueous redox flow batteries. *Joule* 3, 149–163.
- Luo, J., Hu, B., Hu, M., Zhao, Y., and Liu, T.L. (2019b). Status and prospects of organic redox flow batteries toward sustainable energy storage. *ACS Energy Lett.* 4, 2220–2240.
- Luo, J., Sam, A., Hu, B., Debruler, G., Wei, X., Wang, W., and Liu, T.L. (2017). Unraveling pH dependent cycling stability of ferricyanide/ferrocyanide in redox flow batteries. *Nano Energy* 42, 215–221.
- Lund, H. (2007). Renewable energy strategies for sustainable development. *Energy* 32, 912–919.
- Ma, D., Wu, W., Zai, J., Shu, C., Tsega, T.T., Chen, L., Qian, X., and Liu, T.L. (2019). Highly active nanostructured CoS<sub>2</sub>/CoS heterojunction electrocatalysts for aqueous polysulfide/iodide redox flow batteries. *Nat. Commun.* 10, 3367.
- Price, A., Bartley, S., Male, S., and Cooley, G. (1999). A novel approach to utility-scale energy storage. *Power Eng. J.* 13, 122–129.
- Rauh, R.D., Abraham, K.M., Pearson, G.F., Surprenant, J.K., and Brummer, S.B. (1979). A lithium/dissolved sulfur battery with an organic electrolyte. *J. Electrochem. Soc.* 126, 523–527.
- Robb, B.H., Farrell, J.M., and Marshak, M.P. (2019). Chelated chromium electrolyte enabling high-voltage aqueous flow batteries. *Joule* 3, 2503–2512.
- Schrag, D.P. (2007). Preparing to capture carbon. *Science* 315, 812–813.
- Skyllas-Kazacos, M. and Robins, R.G. (1988). US Pat. 4, 786 567.
- Skyllas-Kazacos, M., Cao, L., Kazacos, M., Kausar, N., and Mousa, A. (2016). Vanadium electrolyte studies for the vanadium redox battery—a review. *ChemSusChem* 9, 1512–1543.
- Skyllas-Kazacos, M., Kazacos, G., Poon, G., and Verseema, H. (2010). Recent advances with UNSW vanadium-based redox flow batteries. *Int. J. Energy. Res.* 34, 182–189.
- Skyllas-Kazacos, M., Rychcik, M., Robins, R.G., and Fane, A.G. (1986). New all-vanadium redox flow cell. *J. Electrochem. Soc.* 133, 1057–1058.
- Thaller, L.H. (1976). U.S. Pat. 3, 996 064.
- Wei, X.L., Xia, G.-G., Kirby, B., Thomsen, E., Li, B., Nie, Z., Graff, G.G., Liu, J., Sprenkle, V., and Wang, W. (2015). An aqueous redox flow battery based on neutral alkali metal ferri/ferrocyanide and polysulfide electrolytes. *J. Electrochem. Soc.* 163, A5150–A5153.
- Wei, X., Xu, W., Vijayakumar, M., Cosimbescu, L., Liu, T., Sprenkle, V., and Wang, W. (2014). TEMPO-based catholyte for high-energy density nonaqueous redox flow batteries. *Adv. Mater.* 26, 7649–7653.
- Yang, Z., Tong, L., Tabor, D.P., Beh, E.S., Goulet, M.-A., Porcellinis, D.D., Aspuru-Guzik, A., Gordon, R.G., and Aziz, M.J. (2018). Alkaline benzoquinone aqueous flow battery for large-scale storage of electrical energy. *Adv. Energy Mater.* 8, 1702056–1702064.
- Yang, Z., Zhang, J., Kintner-Meyer, M.C., Lu, W.X., Choi, D., Lemmon, J.P., and Liu, J. (2011). Electrochemical energy storage for green grid. *Chem. Rev.* 111, 3577–3613.
- Yao, Y., Lei, J., Shi, Y., Ai, F., and Lu, Y.-C. (2021). Assessment methods and performance metrics for redox flow batteries. *Nat. Energy* 6, 582–588.
- Ziegler, M.S., Mueller, J.M., Pereira, G.D., Song, J., Ferrara, M., Chiang, Y.-M., and Trancik, J.E. (2019). Storage requirements and costs of shaping renewable energy toward grid decarbonization. *Joule* 3, 2134–2153.
- Zhang, S., Guo, W., Yang, F., Zheng, P., Qiao, R., and Li, Z. (2019). Recent progress in polysulfide redox-flow batteries. *Batteries Supercaps* 2, 627–637.
- Zhao, Y., Ding, Y., Song, J., Peng, L., Goodenough, J.B., and Yu, G. (2014). A reversible Br<sub>2</sub>/Br<sup>-</sup> redox couple in the aqueous phase as a high-performance catholyte for alkali-ion batteries. *Energy Environ. Sci.* 7, 1990–1995.
- Zhou, Y., Cong, G., Chen, H., Lai, N.-C., and Lu, Y.-C. (2020). A self-mediating redox flow battery: high-capacity polychalcogenide-based redox flow battery mediated by inherently present redox shuttles. *ACS Energy Lett.* 5, 1732–1740.

## STAR★METHODS

## KEY RESOURCES TABLE

REAGENT or RESOURCE	SOURCE	IDENTIFIER
Chemicals and reagents		
potassium ferricyanide	Sinopharm Chemical Reagent Co.	CAS#13746-66-2
potassium sulfide	Sinopharm Chemical Reagent Co.	CAS#1312-73-8
potassium chloride	Sinopharm Chemical Reagent Co.	CAS#7447-40-7
carbon felt	Liaoning JinGu Carbon Materials Co.	CAS#NA
Nafion 212 membrane	Ion Power Inc.	CAS#NA

## RESOURCE AVAILABILITY

## Lead contact

Further information and requests for resources and reagents should be directed to and will be fulfilled by the lead contact, Chuankun Jia ([jiachuankun@csust.edu.cn](mailto:jiachuankun@csust.edu.cn)).

## Materials availability

This study did not generate new unique reagents.

## Data and code availability

All data reported in this paper will be shared by the lead contact upon request.

This work is an experimental study of redox flow battery and there is no code generated.

Any additional information required to reanalyze the data reported in this work paper is available from the Lead Contact upon request.

## EXPERIMENTAL MODEL AND SUBJECT DETAILS

The PFRFB cell consisted of three main components: electrolytes, electrodes and membrane. Electrolytes including potassium ferricyanide (AR), potassium sulfide (CP) and potassium chloride (AR). They were received from Sinopharm Chemical Reagent Co., Ltd and used without further purification. Carbon felt (5 mm, carbon >98.8%, bulk density 0.08–0.11 g cm<sup>-3</sup>) was employed as electrodes and purchased from Liaoning JinGu Carbon Materials Co., Ltd.. Nafion 212 membrane (Dupont, DE, USA) was ordered from Ion Power Inc. and pretreated before use. Prior to use, the Nafion 212 membrane was heated in 1.0 M KOH solution at 80°C for 1 hour followed by washing away residual KOH with deionized water at room temperature. The resulting membrane with K<sup>+</sup> conductivity was soaked in deionized water and ready to use.

## METHOD DETAILS

## Cell construction and stack assembly

All operations were conducted at ambient air and room temperature. The proposed neutral PFRFB cell consists of two electrolyte tanks separated from the electrochemical cell, two current collectors, two carbon felts with the geometrical area of 13.5 cm<sup>2</sup> (3.5 cm × 4 cm) as electrodes and a piece of Nafion 212 as cation-exchange membrane in the cell. Catholyte with three different concentrations (K<sub>3</sub>[Fe(CN)<sub>6</sub>]: 0.1 M, 0.5 M and 0.8 M) and anolyte with 2.0 M K<sub>2</sub>S were obtained by dissolving K<sub>3</sub>[Fe(CN)<sub>6</sub>] and K<sub>2</sub>S in 2.0 M and 1.0 M KCl solution, respectively. The cell employs a 25.0 mL solution of 0.1 M K<sub>3</sub>[Fe(CN)<sub>6</sub>] in 2.0 M KCl as catholyte and a 15.0 mL solution of 2.0 M K<sub>2</sub>S in 1.0 M KCl as anolyte for cell performance tests, unless otherwise specialized. Both catholyte and anolyte were pumped between the storing tank and the corresponding compartment of the electrochemical cell by a peristaltic pump (Williamson Manufacturing Co., Ltd, UK).

A cell stack consisting of 10 single cells, each with the geometric area of  $1700\text{ cm}^2$  ( $100\text{ cm} \times 17\text{ cm}$ ), was assembled to verify the scalability and performance of the polysulfide/ferricyanide redox combination. A 20.0 L solution with 0.3 M  $\text{K}_3[\text{Fe}(\text{CN})_6]$  in 1.0 M KCl worked as the catholyte while a same volumetric solution of 1.0 M  $\text{K}_2\text{S}$  in 1.0 M KCl served as the anolyte. Electrodes and membrane materials in the stack are the same as in the single cell except for with larger geometric area.

### Electrochemical characterizations

CV measurements were performed using a three-electrode cell configuration with carbon felt ( $1.0\text{ cm} \times 1.0\text{ cm}$ ) as the working electrode, a platinum mesh as the counter electrode and an Ag/AgCl (3.0 M KCl) reference electrode as the reference electrode at a VSP BioLogic workstation. The charging-discharging cycling of single cell was carried out under galvanostatic mode on a LAND battery testing system (CT2001A) at  $20\text{ mA cm}^{-2}$  within a voltage range of 0.4–1.4 V. Rate performance was conducted under current densities from  $20\text{ mA cm}^{-2}$  to  $140\text{ mA cm}^{-2}$  with an increase of  $20\text{ mA cm}^{-2}$  and then back to  $20\text{ mA cm}^{-2}$ . For each applied current density, the cell ran 5 charging-discharging cycles and CE, EE, and VE were recorded. Polarization curves of cells with different electrolyte combinations were obtained from an Arbin instrument (BT-I) at 100% SOC. The measurements ended when either the voltage reached to 0 V or the current exceeded over 10 A. The charging-discharging cycling tests of the stack were completed by NEWARE Battery Testing System (CT-4002-60V40A-NA).

### QUANTIFICATION AND STATISTICAL ANALYSIS

The electrochemical original data were collected on a VSP BioLogic workstation, a LAND battery testing system (CT2001A), an Arbin instrument (BT-I), and an NEWARE Battery Testing System (CT-4002-60V40A-NA), separately. Figures were produced by Origin from raw data.

### ADDITIONAL RESOURCES

Any additional information about the cell assembly, tests and data reported in this paper is available from the lead contact on request.